Available online at
https://jcrinn.com/
https://crinn.conferencehunter.com/

Journal of Computing Research and Innovation 11(2) 2026

Journal of Computing Research and Innovation

Radiomic and Interpretable Machine Learning for Non-Invasive Classification of Histological Subtypes of Non-Small Cell Lung Cancer

Christy Ntambwe Kabamba[1*], Tacite Mazoba Kpanya[2], Pierre Kafunda Katalayi[3], Angel Torrado-Carvajal[4], Eugène Mbuyi Mukendi[5]

[1,3,5]*Department of Mathematics, Statistics and Computer Science, Faculty of Science and Technology, University of Kinshasa, Kinshasa, Democratic Republic of Congo.*
[2]*Medical Imaging Department, Faculty of Medicine, University of Kinshasa, Kinshasa, Democratic Republic of Congo.*
[4]*Medical Image Analysis and Biometry Laboratory, Universidad Rey Juan Carlos, Madrid, Spain.*

ARTICLE INFO

Article history:
Received 9 January 2026
Revised 12 August 2026
Accepted 14 August 2026
Online first
Published 1 September 2026

Keywords:
Radiomics
Adenocarcinoma
Squamous Cell Carcinoma
Explainability
Random Forest

DOI:
10.24191/jcrinn.v11i2.593

ABSTRACT

Telling apart the main histological subtypes of non-small cell lung cancer (NSCLC), like adenocarcinoma (ADC) and squamous cell carcinoma (SCC), is key for guiding treatment and making personalized medicine better. This study looks to build and test an interpretable machine learning model using radiomic features pulled from 3D CT scans. A retrospective cohort of 527 patients with non-small cell lung cancer (344 men and 183 women) was analyzed and randomly divided into a training set (75%) and a test set (25%). A total of 1,409 radiomic features were extracted from CT images. Three feature selection methods were evaluated, and class rebalancing using the SMOTE technique was applied only to the training set. Several classifiers, including random forest, were trained to distinguish adenocarcinoma from squamous cell carcinoma. Model performance was evaluated using the area under the ROC curve (AUC), precision and sensitivity, while interpretability was ensured using the SHAP (Shapley Additive Explanations) method. The consensus feature selection method, which was the best, selected 17 features for the SCC class and 13 for ADC. The Random Forest model stood out from seven other classifiers with superior performance in predicting ADC and SCC, with AUC values of 0.937 and 0.907, accuracy of 0.891 and 0.774, and sensitivity of 0.755 and 0.889, respectively. This study shows that CT-based radiomics combined with an interpretable Random Forest model allows reliable discrimination between ADC and SCC in NSCLC. SHAP analysis improves understanding of the decision-making process and supports the clinical applicability of the model.

[1*]Corresponding author. E-mail address: nchristy34@gmail.com

https://doi.org/10.24191/jcrinn.v11i2.593

1. INTRODUCTION

Lung cancer is a very dangerous disease that compromises the health and functioning of the lungs, potentially leading to a significant decrease in respiratory capacity. As one of the leading causes of cancer-related deaths worldwide, with the highest mortality rates in both sexes (Sung et al., 2021), this cancer has different histological subtypes with different clinical behaviors and outcomes (Robertson et al., 2024). Histologically, this cancer is divided into two families: non-small cell lung cancer (NSCLC), accounting for approximately 85% of diagnosed cases, and small cell lung cancer (SCLC) (Nicholson et al., 2021). In most cases, this cancer is diagnosed at an advanced stage in the majority of patients, which significantly weakens the prognosis for survival. According to the classification criteria established by the WHO, adenocarcinoma (ADC) and squamous cell carcinoma (SCC) are currently the most common histological subtypes of the first group in clinical practice (Nicholson et al., 2021). Accurate and timely identification of histological subtypes and molecular alterations is essential to providing patients with the best possible treatment, and molecular analysis is now a central part of lung carcinoma management, with direct clinical implications (Pusztaszeri et al., 2011). Conventional approaches to the accurate diagnosis of this disease are based on the analysis of pathological tissue samples taken during a lung biopsy, which is an invasive procedure that requires considerable resources (Kim & Shin., 2017). Although pathological analysis makes it possible to determine the precise type of bronchial cancer, how far the cells have spread, their aggressiveness and their characteristics, it "places a physical and economic burden on the patient due to the risks of lung surgery, the postoperative recovery time and the additional care required" (Kim & Shin., 2017). In addition, the information obtained from the biopsy only concerns the area where the sample was taken, which raises the issue of the representativeness of the tumor tissue sample. Obviously, depending on where the tumor sample was taken, the mutational burden of a lesion will not be the same and therefore cannot accurately characterize the entire tumor (Dirand, 2020). In addition to this spatial limitation, the temporal aspect of biopsy also poses a problem. The sample is taken before treatment but is not usually repeated during treatment due to its invasive nature. However, it has been proven that the biological parameters of tumors can change over time in response to treatment (Pusztaszeri et al., 2011, Dirand, 2020). Given the limitations of conventional methods, new technologies are being considered to automatically assist clinicians in the accurate classification of histological subtypes of lung cancer using a noninvasive, effective, and clinically applicable approach.

Medical imaging, particularly computed tomography (CT), is a non-invasive, rapid, and cost-effective approach to the diagnosis of bronchial cancer (Hoffman et al., 2020). The images produced by this modality contain visual information closely related to histological expression, thus enabling the differentiation of tumor subtypes (Eldho & Nithyanandh, 2024). While radio diagnostics interpretation has historically been based on the qualitative analysis of images of the object under study, the last decade has seen the emergence of radiomics (Lambin et al., 2012), a field of research that attempts to identify new quantitative biomarkers that are not immediately apparent to the naked eye in routine medical imaging. As a result, while the detection and classification of lung nodule malignancy has been extensively studied, the classification of histological subtypes, particularly ADCs and SCCs, driven by the rise of radiomics and deep learning, is gradually emerging. Radiomics is a powerful method of quantitative analysis of medical images aimed at extracting numerical characteristics that can be used for clinical prediction and classification. It highlights relevant relationships between medical images and tumor phenotypes (Dirand, 2020). The deployment of these characteristics as input for machine learning algorithms has the potential to significantly improve the accuracy and efficiency of diagnosis, due to their ability to process large data sets. Numerous studies have thus demonstrated the value of radiomics and machine learning in the histological diagnosis of lung cancer (Alahmari et al., 2018; Esfahani et al., 2022). In 2021, Guo et al. (2021) implemented two models (ProNet and com_radNet) based on CT images and obtained respective AUCs of 0.840 and 0.789, and corresponding sensitivities of 81.3% and 83.8% for separating ADC and SCC. Similarly, Song et al. (2023) demonstrated the effectiveness of intensity, texture (Gray Level Co-occurrence Matrix (GLCM), Gray Level Run Length Matrix (GLRLM), Gray Level Size Zone Matrix (GLSZM)) and filtered image features

https://doi.org/10.24191/jcrinn.v11i2.593

in differentiating between ADC and SCC. In their experiment, ensemble learning algorithms demonstrated better generalization performance ($p = 0.00418$) than other non-ensemble algorithms. The Bagging-AdaBoost-SVM model obtained AUC values of 0.815 and 0.737 for SCC and ADC, respectively, on the test set. In a retrospective study in 2024 involving 317 patients, Kuang et al. (2024) developed interpretable models to predict three histological subtypes of NSCLC (ADC, SCC, LCC (Large Cell Carcinoma)) from radiomic signatures specific to each subtype. 9, 12, and 8 key radiomic features were selected for the ADC, SCC, and LCC groups, respectively. In terms of performance, the XGB model demonstrated superior performance in predicting SCC and LCC, with AUC values of 0.789 and 0.848, respectively. For ADC prediction, Random Forest excelled, with an AUC of 0.748. In 2025, Solodkiy et al. (2025) generated 1,029 radiomic features from lung lesions and reduced their dimensionality to 247. The SLS model they proposed achieved an average classification accuracy of 0.86 on the test set. Remaining focused on two histological types, Selvam et al. (2024), in their very recent study of a cohort of 46 ADCs and 28 SCCs, extracted 101 features and used several classifiers. The results show that MLP with activation (ReLu) achieved 83% accuracy and 86% sensitivity in distinguishing SCC from ADC.

In addition, several recent studies have used a combination of tumor markers, clinical information, and radiomic features to implement models for predicting histological subtypes of NSCLC. Yan and Wang (2020) developed predictive models based on PET alone, CT alone, and the combination of PET+CT, and showed that the combined PET–CT model offered the best performance for predicting ADC, SCC, and metastases in NSCLC. Zhao et al. (2025) selected thirteen different characteristics, including nine radiomic characteristics, two clinical characteristics (gender and smoking status), and two biological markers (CEA and SCCA), and obtained an AUC of 0.910 on the test set.

Finally, a few studies using deep learning as an approach have demonstrated the ability to predict subtypes: Liang et al. (2024) developed a 3D CNN model for automatic feature extraction from computed tomography (CT) images. The results show that their proposed model achieved 0.88 accuracy and 0.89 area under the receiver operating characteristic curve (AUC) when distinguishing between lung adenocarcinoma (ADC) and lung squamous cell carcinoma (SCC), indicating the potential for a noninvasive method to predict histological subtypes of lung cancer. Similarly, Marentakis et al. (2021) combined InceptionResNetv2 with an LSTM (Long Short-Term Memory) network to merge information related to the spatial consistency of CT slices of the tumor. The result shows that they improved accuracy and area under the ROC curve, which are 0.74 and 0.78, respectively, compared to their previous study, thus outperforming experts by 7 to 25% ($p < 0.05$).

It should be noted that, although previous work has demonstrated the potential of radiomic features in the non-invasive classification of histological subtypes of non-small cell lung cancer, particularly adenocarcinomas and squamous cell carcinomas, it suffers from the problem of data imbalance. This has probably and potentially skewed the results of the models in favor of the most heavily represented classes (Tang et al., 2025).

Furthermore, most of these studies focus on the predictive performance of the models and do not evaluate the interpretability of radiomic models, which complicates the explainability of the decisions produced. In this article, we first propose a consensus-based feature selection approach based on the intersection of feature sets from RFE + Random Forest and RFE + XGBoost. We subsequently used the intraclass correlation coefficient (ICC) to ensure that the sets of features selected by consensus for each class were the most robust across all imaging systems. We built machine learning models based on specific radiomic features selected by consensus to predict the histological subtypes of NSCLC (ADC and SCC) in a non-invasive and accurate manner. Finally, we address the issue of class imbalance and model interpretability through appropriate strategies to ensure robust and reliable performance and improve model interpretability using the SHapley Additive exPlanations (SHAP) method.

https://doi.org/10.24191/jcrinn.v11i2.593

2. MATERIALS AND METHOD

This section describes the datasets and the proposed radiomic pipeline, including CT image preprocessing, radiomic feature extraction and selection, class imbalance management, and supervised classification of NSCLC histological subtypes. Fig. 1 presents an overview of the proposed method.

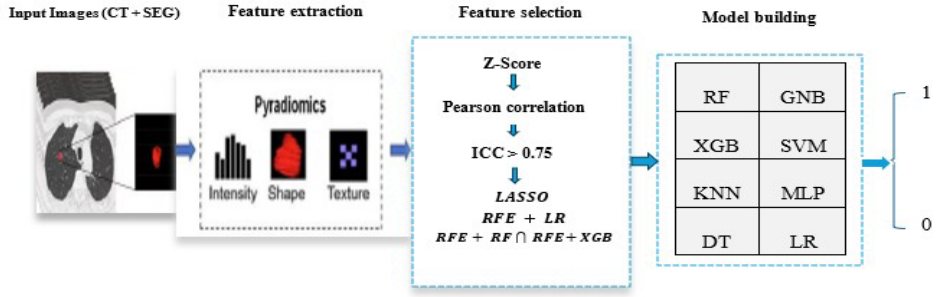

Fig. 1. Proposed radiomic pipeline for automated classification of NSCLC histological subtypes from CT images

Source: Authors' work

2.1 Data acquisition

Two retrospective datasets on non-small cell lung cancer, one local and one public, were used in this study. For the local study, data were collected retrospectively from 342 patients with non-small cell lung cancer who had CT scans from April 2016 to December 2024 at three major healthcare facilities in Kinshasa, the capital of the Democratic Republic of Congo (Cliniques Universitaires de Kinshasa, Centre Hospitalier Mère et Enfant de Monkole, and Centre Hospitalier Diamant de Kinshasa), and for whom clinical data and diagnosis were available. These data consist of manual segmentation and cross-sections. 324 out of 342 cases contain complete segmentation annotations of the tumor region and histological diagnosis, including 221 cases of adenocarcinoma, 103 cases of squamous cell carcinoma, and 18 cases of other histological types. This collection was approved by the National Health Ethics Committee of the Democratic Republic of Congo, under reference number N°620/CNES/BN/PMMF/2025 dated 20/01/2025, in the appendices.

The other dataset is NSCLC Radiomics (Aerts et al., 2014), which is one of the main public medical imaging databases dedicated to the study of non-small cell lung cancer. It is hosted on The Cancer Imaging Archive (TCIA) platform and is the result of the LIDC-IDRI (Armato III et al., 2011). It includes CT images from 422 patients with non-small cell lung cancer, as well as segmentation of different tissues such as lung lobes, pulmonary effusions, and tumor lesions, clinical information such as age and race, histological information; and patient survival status. Among them, 421 cases are annotated with segmentation of tumor lesion areas, and 380 cases have histological records clearly confirmed by pathological sections, of which 51 are adenocarcinomas, 152 are squamous cell carcinomas, 114 are large cell carcinomas, and 63 are unspecified.

Finally, after eliminating invalid data for the study, our sample included 524 patients, including 271 with adenocarcinoma and 253 with squamous cell carcinoma. DICOM RTSTRUCT and DICOM-SEG files were used to define regions of interest (ROIs) on CT images, based on manual segmentations performed by experienced radiation oncologists and radiologists targeting histological subtypes of NSCLC.

https://doi.org/10.24191/jcrinn.v11i2.593

2.2. Pre-processing

The pre-processing of CT images involved several essential steps to prepare the data for analysis (Fadzli et al., 2024). First of all, the original CT images were acquired in DICOM format. We first converted these images to NIfTI format using SimpleITK, while preserving the original voxel intensity information. These CT intensities were expressed in Hounsfield units (HU), with the conversion of pixel values stored in HU performed according to the DICOM Rescale Slope and Rescale Intercept parameters. The resulting CT volumes were then cropped using the corresponding segmentation masks to retain only the lung region. Next, the voxel intensities were limited to the range of -1000 to 400 HU and normalized between [0,1] using min–max normalization. The volumes were resized to the required dimensions, and Gaussian smoothing was applied with SimpleITK to reduce image noise. All preprocessing steps were performed in Python using SimpleITK, pydicom and NumPy.

2.3. Feature extraction and selection

Radiomic features describe medical images and enable machine learning algorithms to effectively differentiate histological subtypes and provide quantitative indicators of tumor phenotype. Careful selection of features facilitates the identification of essential discriminating information, while reducing the complexity of the learning process and increasing predictive efficiency (Van Griethuysen et al., 2017; Zwanenburg et al., 2020).

Radiomic features to be extracted from CT images are classified into three categories: shape features, which describe the geometry of the region of interest and help to understand the physical dimensions and shape irregularities of the tumor mass. Intensity or first-order statistical features, which describe the statistical distribution of voxels within the ROI, providing information on the density and uniformity of tumor tissue via measures such as mean, median, variance, standard deviation, skewness, kurtosis, percentiles, energy, entropy, etc. Texture features utilize co-occurrence matrix and other statistical models to quantify the spatial heterogeneity of intensities within the tumor region, thus providing a comprehensive view of the tumor's textural patterns and essential information about its pathophysiological state. Thus, radiomic features were extracted from the original CT images and pre-processed images using the PyRadiomics library, as illustrated in Fig. 2. From the original images, a set of 107 features, including first-order statistics, shape descriptors, and texture features, was extracted. Only first-order statistics and texture features (93) were extracted from the filtered images, as shape features are independent of grey-level distribution and therefore do not exhibit relevant variations after filtering.

Thus, shape features were extracted exclusively from the original images, while first-order and texture features were calculated from both the original and pre-processed images. The complete set of extracted features consists of 1,409 features per lesion, which necessitated a pre-processing and dimension reduction step. After the extraction step, the raw radiomic vectors exhibited high redundancy, heterogeneous scales between features, outliers and missing values. To this end, systematic pre-processing was applied, including the removal of 26 features that were constant and/or had a high rate of missing or undefined values (NaN) in the training set, followed by z-score normalization per feature. The same pre-processing parameters were also applied to the test set to ensure consistency and the absence of information leakage.

https://doi.org/10.24191/jcrinn.v11i2.593

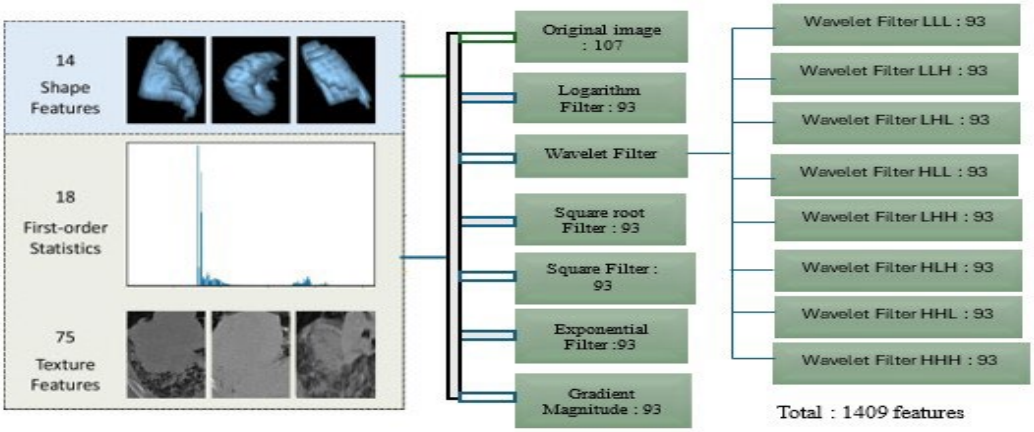

Fig. 2. Radiomic features extracted from original and filtered CT images

Source: Author's work

Given the high number of features (1,383) and the limited number of patients in the study, direct use of all these features would lead to a major risk of overfitting. Radiomic feature selection was performed in a class-oriented manner. Two independent pipelines were constructed, one dedicated to the detection of adenocarcinoma and the other to the detection of squamous cell carcinoma. A combination of univariate statistical tests, penalized supervised methods, and stability-based selection was used to identify radiomic signatures specific to each histological subtype.

Thus, for each pipeline, a two-step approach (filtering + selection) was implemented. For filtering, pairs of features with high correlation ($|r| > 0.9$) were considered redundant, and one feature per pair was removed based on its variance or univariate discriminative power. Three methods were tested for feature selection: Lasso, recursive feature elimination combined with the logistic regression algorithm (RFE+LR), and finally, a consensus selection based on the intersection of the feature sets obtained by RFE + Random Forest and RFE + eXtreme Gradient Boosting (RFE + RF ∩ RFE + XGB). This strategy consists of retaining only the features selected simultaneously by both methods. The objective was therefore to reduce the bias associated with a single algorithm, eliminate unstable features, and enhance the reliability of the selected radiomic biomarkers.

2.4. Data imbalance management and classification

As our dataset was imbalanced, with 255 adenocarcinomas versus 272 squamous cell carcinomas, we used the SMOTE method (Tang et al., 2025) to increase the data in the minority class. SMOTE generates synthetic samples by interpolating between samples and neighbors until the classes are balanced. SMOTE is applied only to the training data to avoid skewing the test cohort. In order to identify radiomic signatures specific to each histological subtype, two detection-oriented binary classification models were developed: one model dedicated to the detection of adenocarcinoma (ADC) and a second dedicated to the detection of squamous cell carcinoma (SCC). This approach allows for an explanatory analysis of the discriminating radiomic characteristics specific to each entity.

We trained eight different machine learning algorithms to ensure that our predictions were reliable. These algorithms included: support vector machine (SVM), K-nearest neighbors (KNN), decision tree (DT), Logistic Regression (LR), Gaussian Naive Bayes (GNB), logistic regression (LR), multilayer perceptron (MLP), Random Forest and XGBoost (XGB). Each algorithm learns in a specific way, allowing

https://doi.org/10.24191/jcrinn.v11i2.593

us to understand the hidden relationships between radiomic features and histological subtypes. As such, SVM is effective in high-dimensional spaces (Rastogi et al., 2022), KNN is particularly effective for similarity-based classification, based on local relationships between features (Hu et al., 2018). DT for defining clear decision rules that can be interpreted in the form of hierarchical structures (Loh, 2011), LR measures the association between the occurrence of an event (qualitative dependent variable) and the factors likely to influence it (explanatory variables) (Rastogi et al., 2022), GNB for estimating the probability of a sample belonging to a class, calculated from the Gaussian density of each feature (Shukri et al., 2024). MLP allows non-linear and complex relationships to be captured (Kabamba et al., 2019), (Fadzli et al., 2024), RF for ensemble learning improves model generalization while reducing overfitting (Rastogi et al., 2022), and finally XGB is effective at managing complex data thanks to its advanced gradient boosting strategies (Chen & Guestrin, 2016). Model training is performed on the training sample using 10-fold stratified cross-validation, repeated 5 times, allowing performance to be estimated in terms of accuracy, sensitivity, specificity, precision, F1-score and area under the curve (AUC). The hyperparameters for each classifier were selected using a strategy combining prior experience from the literature and systematic optimization through cross-validation. GridSearchCV was used with five-fold stratified cross-validation and AUC as the performance metric.

3. RESULTS

3.1 Patients and implementation details

A total of 545 patients diagnosed with non-small cell lung cancer (NSCLC), coming from local and public sources, including 342 from the three reference hospitals in Kinshasa and 203 from the NSCLC Radiomics dataset [22], were collected for the study. Among them, 21, or 3.9%, from the local source were excluded from the study: 13 had no segmentation in their records; 5 had no information on the histological diagnosis; and 3 had significant artifacts. In the end, 524 patients were eligible, including 271 (51.7%) ADC cases and 253 (48.3%) SCC cases. Twenty-five percent (25%) of the patients were set aside for an independent test set, used exclusively for the final evaluation of the models. The remaining 75% made up the development set, where the training and validation of the models took place. The initial characteristics of the studied population, including demographic data, clinical stage, and key clinical parameters collected during data gathering, as well as the distribution of patients across the different sets, are shown in Table 1.

The study population had a mean age of 66 years, consistent with epidemiological trends for non-small cell lung cancer worldwide, and showed a male predominance (sex ratio = 1.88). The T, N and M stages describe local tumor spread, lymph node involvement, and the presence of metastases, respectively, and their combination determines the overall stage of the disease. The comparison between the training and test sets was performed using parametric tests. It goes without saying that the majority of parameters do not show a statistically significant difference ($p > 0.05$), indicating good homogeneity between the two sets.

In terms of implementation, our experiments were conducted on Windows with an Intel® Core™ i77700 processor with 16GB of RAM, using Python 3.10.11 with PyRadiomics for feature extraction and scikit-learn/XGBoost for the implementation of the eight classifiers evaluated, while class imbalance was addressed using the imblearn package, in particular via oversampling techniques (SMOTE).

https://doi.org/10.24191/jcrinn.v11i2.593

Table 1: Characteristics of ADC and CSC subjects according to training and test samples

	Total N = 524	Train N = 393 (75%)	Test N = 131 (25%)	P-value
Age	66.0 [60.0–73.0]	66.0 [60.0–73.0]	67.0 [61.0–74.0]	0.684
T_stage				0.721
1	91 (17.4%)	68 (17.3%)	23 (17.6%)	
2	210 (40.1%)	155 (39.4%)	53 (40.5%)	
3	115 (21.9%)	88 (22.4%)	28 (21.3%)	
4	107 (20.4%)	82 (20.9%)	26 (19.8%)	
5	1 (0.2%)	0 (0.0%)	1 (0.8%)	
N_stage				0.463
0	181 (34.5%)	134 (34.1%)	47 (35.9%)	
1	42 (8.0%)	32 (8.4%)	10 (7.6%)	
2	184 (35.1%)	139 (35.3%)	45 (34.4%)	
3	101 (19.3%)	77 (19.5%)	24 (18.3%)	
4	16 (3.1%)	11 (2.7%)	5 (3.8%)	
M_stage				0.042*
0	502 (95.8%)	380 (96.7%)	122 (93.1%)	
1	22 (4.2%)	13 (3.3%)	9 (6.9%)	
Stage				0.377
I	76 (14.5%)	58 (14.7%)	18 (13.7%)	
II	60 (11.5%)	45 (11.5%)	15 (11.5%)	
IIIa	158 (30.1%)	117 (29.8%)	41 (31.3%)	
IIIb	230 (43.9%)	173 (44.0%)	57 (43.5%)	
Histology				0.498
ADC	271 (51.7%)	204 (51.9%)	67 (51.1%)	
SCC	253 (48.3%)	189 (48.1%)	64 (48.9%)	
Gender				0.553
Female	181 (34.5%)	136 (34.6%)	45 (34.4%)	
Male	343 (65.5%)	257 (65.5%)	86 (65.6%)	

Source: Authors' own analysis

3.2 Results of radiomic feature extraction and selection

One thousand four hundred and nine (1409) radiomic features were extracted from the original and filtered images, including a wide range of shape, intensity, and texture features. For selection, we filtered out 26 features with low variance and/or a high rate of missing or undefined values (NaN), resulting in 1,383 features. We then applied three feature selection methods separately to significantly reduce the size of the input vector for the algorithms:

1) LASSO allowed us to select 187 features for ADC and 141 for SCC.
2) Recursive feature elimination combined with logistic regression (RFE + LR) identified 37 and 39 features for ADC and SCC, respectively.
3) The third method, which consists of a consensus feature selection strategy, identified 13 and 17 consensus features for ADC and SCC, respectively.

The SMOTE method was applied only to the training set during ten-fold stratified cross-validation in order to balance the ADC and SCC classes, while preserving the independence of the test set.

3.3 Predictive performance results of the different models

The main prediction results of our two models (one for ADC and the other for SCC) on the training and test sets, with eight classifiers, are presented in Fig. 3 and Fig. 4. Due to space limitations, the performances are listed according to the best feature selection approach used in the study.

https://doi.org/10.24191/jcrinn.v11i2.593

3.3.1 Prediction of lung adenocarcinoma

During the implementation of the lung adenocarcinoma (ADC) prediction model, eight classifiers were trained and tested. Following a detailed comparison of the machine learning models associated with different feature selection methods for ADC prediction, the Random Forest model with consensus feature selection achieved the best overall performance across all evaluation metrics. It achieved an AUC of 0.937 (95% CI: 0.924–0.950), an accuracy of 0.851, a sensitivity of 0.755, a precision of 0.892, and an F1-score of 0.818 on the test set, demonstrating its robustness. The model also performed well during training, achieving an accuracy of 0.929, a sensitivity of 0.780, a precision of 0.860, and an AUC of 0.964 (95% CI: 0.964–0.966), reflecting its effective learning capability.

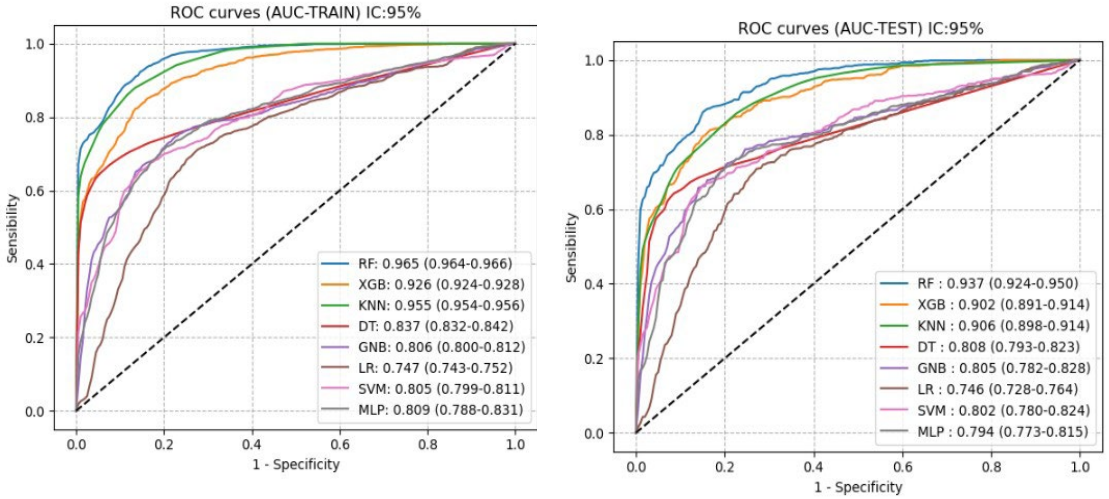

Fig. 3 - ROC curves and AUC values for ADC prediction using the consensus method

Source: Authors' own analysis

3.3.2 Prediction of squamous cell carcinoma

The same eight classifiers were trained and tested on the SCC group features using the three feature selection methods. Once again, the Random Forest model with consensus features achieved the best overall performance across all evaluation metrics. It achieved an accuracy of 0.789, a sensitivity of 0.889, a precision of 0.814, an F1-score of 0,850, and an AUC of 0.907 (95% CI: 0.892–0.922) on the test set. The model also performed well during training, achieving an accuracy of 0.782, a sensitivity of 0.904, a precision of 0.826, and an AUC of 0.932 (95% CI: 0.931–0.933), demonstrating its effective learning capability.

https://doi.org/10.24191/jcrinn.v11i2.593

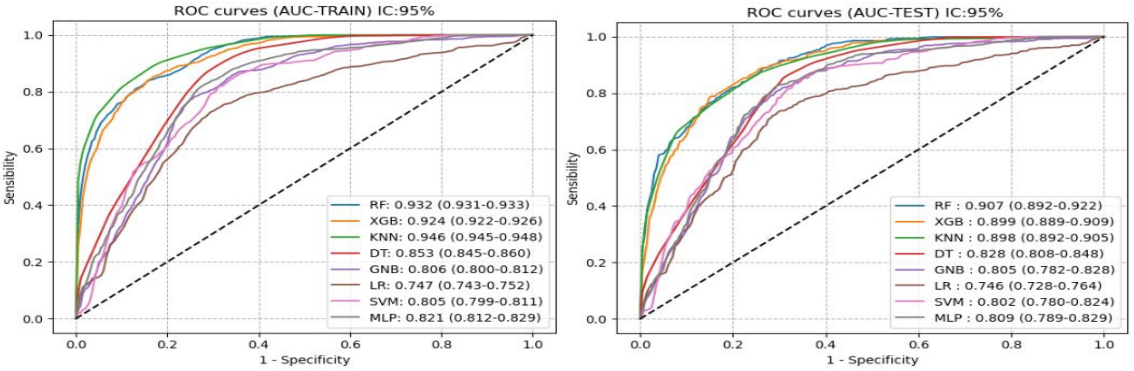

Fig. 4. - ROC curves and AUC values for SCC prediction using the Consensus method

Source: Authors' own analysis

It should be noted that after training these eight classifiers, a comparative evaluation was carried out on the test set. Fig. 5 summarizes the predictive performance of these eight classifiers for ADC and SCC using the features selected by consensus.

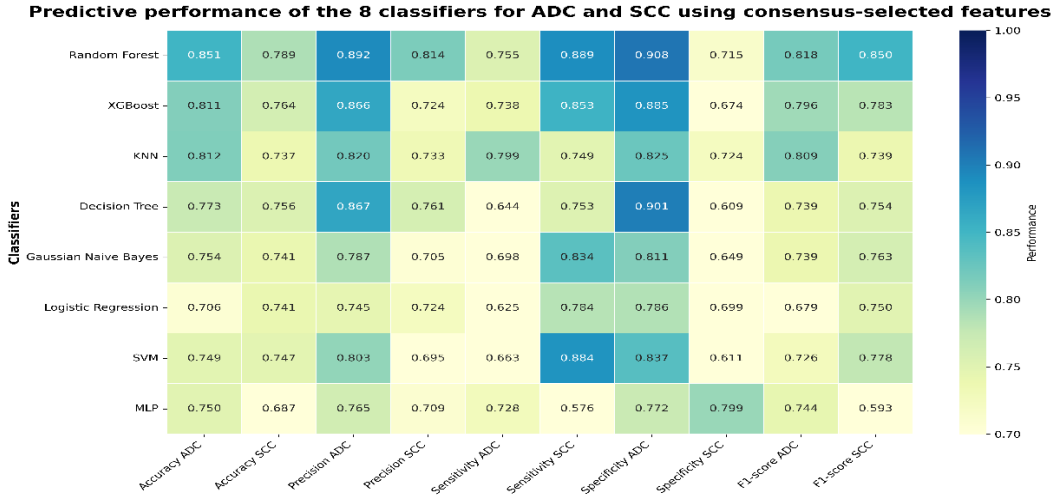

Fig. 5. - ADC and SCC prediction performance based on several metrics

Source: Authors' own analysis

At the same time, a comparison matrix using p-values according to DeLong's test was calculated in order to estimate the significance of the difference between one classifier and the others. Therefore, for a value of $p \geq 0.05$, the difference is not statistically significant. Thus, although some classifiers had neighboring AUCs, only those with $p < 0.05$ are considered better with a sufficient confidence interval. In view of all these tests, the KNN classifier showed significantly high deviations, indicating a risk of overfitting, and the RF classifier appeared more balanced for predicting ADC and SCC, offering the best average performance while maintaining good generalization capacity and showing significant differences

https://doi.org/10.24191/jcrinn.v11i2.593

compared to several other competing classification classifiers. Based on these observations, it was selected as the final model for studying the explainability of the models.

3.3.3 Explanation of models with SHapley Additive exPlanations (SHAP) method

The RF model based on consensus features, which showed the best prediction for differentiating adenocarcinoma from squamous cell carcinoma and vice versa, was used to demonstrate the SHAP diagrams. Thus, Fig. 6 (left and right) shows the overall importance of the 17 and 13 radiomic features consensually selected for the SCC and ADC groups, respectively. The three most important features were exponential_glszm_LowGrayLevelZoneEmphasis, exponential_glszm_ZoneEntropy, and exponential_ngtdm_Coarseness for SCC. Exponential_glszm_LowGrayLevelZoneEmphasis, wavelet-LLH_firstorder_MeanAbsoluteDeviation, and original_firstorder_90Percentile for ADC.

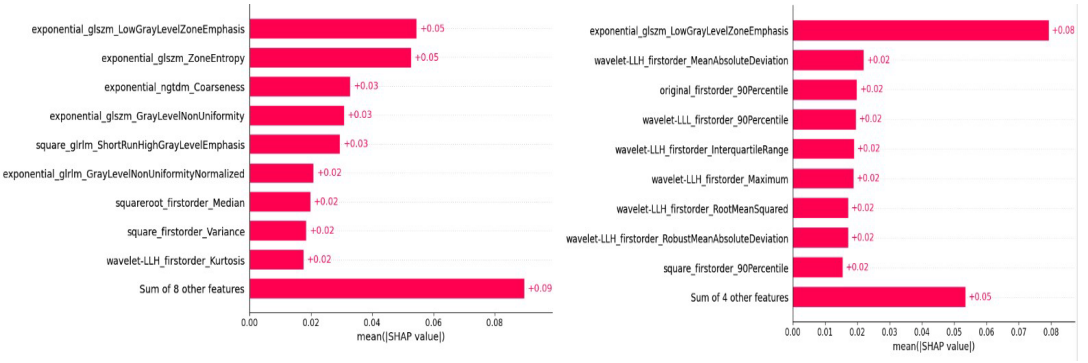

Fig. 6. Overall importance of SCC (left) and ADC (right) characteristics

Source: Authors' own analysis

The decision-making process of the RF model for two randomly selected patients is described using the SHAP strength diagram (Fig. 7 A and B for the SCC group and C and D for ADC). Through these graphs, we can show for a given patient how each characteristic pushes the model's decision towards one class or the other.

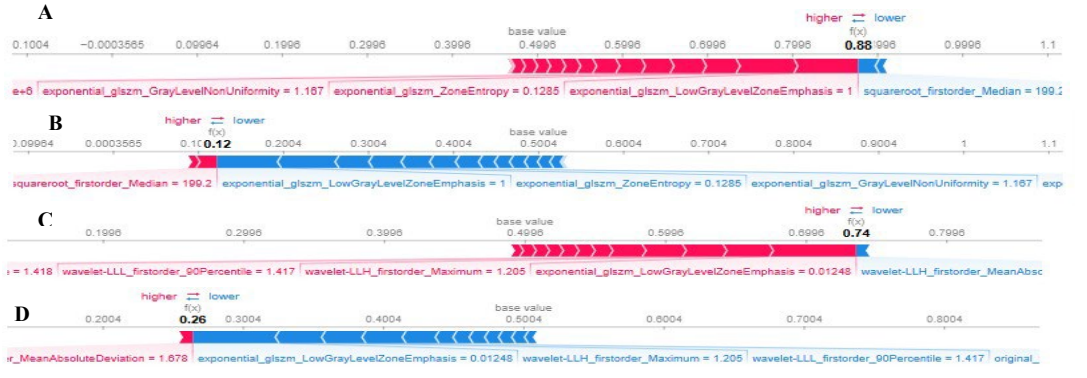

Fig. 7. SHAP strength diagrams for SCC prediction (A, B) and ADC prediction (C, D)

Source: Authors' own analysis

https://doi.org/10.24191/jcrinn.v11i2.593

It can be seen in A that the prediction of our RF model is approximately 0.88, which is above the baseline value of 0.5. The features in red pull the prediction upwards, i.e. towards 1, which is the positive class, in particular: exponential_glszm_GrayLevelNonUniformity (1.187), exponential_glszm_ZoneEntropy (0.1285), exponential_glszm_LowGrayLevelZoneEmphasis (1). On the other hand, a single feature (in blue): squareroot_firstorder_Median (199.2) pushes the prediction slightly downwards, but its effect remains weak. In B, the prediction is around 0.12, even below the baseline value. This time, the blue features dominate and pull the output down, while the red feature (squareroot_firstorder_Median = 199.2) goes in the opposite direction, but its effect also remains very weak. In C, the red features pull the prediction towards the ADC, which is the positive class here, to a value of 0.74, which is also above the baseline value. Finally, in D, the wavelet-LLH_firstorder_MeanAbsoluteDeviation feature (1.678) attempts to pull towards class 0, but its effect also remains very weak. Thus, interpretability analysis based on the SHAP method revealed distinct radiomic signatures for ADC and SCC. The prediction of ADC depends mainly on global intensity characteristics and order 1 statistics, especially after wavelet transformation. This shows a relatively homogeneous and structured grey level distribution. The exponential_glszm_LowGrayLevelZoneEmphasis feature stands out as the main discriminating factor, highlighting the importance of low intensity areas in identifying ADC. In contrast, SCC prediction is dominated by complex textural features derived from GLSZM, GLRLM and NGTDM matrices. This reflects marked intratumorale heterogeneity and a more disordered spatial organization. Features related to entropy, grey level non-uniformity and texture granularity show the highest contributions. This indicates that structural complexity is a key element of the radiomic signature of SCC. These results show that our RF model uses different decision-making mechanisms depending on the histological subtype. It combines global intensity information for ADC and textural properties for SCC. This complementarity reinforces the importance of the radiomic approach for the non-invasive characterization of histological subtypes of bronchial cancer.

4. DISCUSSION

This retrospective study demonstrates the significant potential of radiomics to improve the accuracy of diagnosing malignant lung nodules, particularly in differentiating between ADC and SCC of the lung from CT images, and to inform personalized treatment strategies. By providing quantitative information that complements conventional visual assessment, radiomics improves diagnostic interpretation and also offers a non-invasive approach to enriching visual data from medical imaging, particularly computed tomography.

Today, the accurate identification of either histological subtype in patients with non-small cell lung cancer has major implications for both clinical treatment strategies and the prognosis of these patients. In our study, given the availability of local data collected in three healthcare facilities in the city of Kinshasa, only patients diagnosed with ADC and SCC were included, to which public data from the NSCLC Radiomics database (Aerts et al., 2014) were added. Several feature selection methods were tested, such as LASSO, RFE + LR, and$RFE + RF \cap RFE + XGB$). Fig. 6 illustrates the importance of the features derived from the consensus method, A for SCC and B for ADC. These consensually selected features performed best with the majority of classifiers used and included first-order statistical descriptors and textural features, which are among the most important for differentiating SCC from lung ADC, in line with previous studies (Alahmari et al., 2018, Linning et al., 2019, Selvam et al., 2024, Zhao et al., 2025). In addition, several machine learning models based on the extracted and preselected radiomic features were implemented and compared. The RF model based on the consensus features achieved the best performance for discriminating between ADC and SCC, with a sensitivity and AUC value for the test set of 0. 0.755, 0.937 with CI (0.924–0.950) and 0.889, 0.907 CI (0.892–0.922), respectively. These results outperform the models based on features selected by LASSO (AUC: 0.843 for RF and 0.867 for XGB) and by RFE + LR (AUC: 0.864 and 0.896 for RF). Our model showed a moderate train-test gap (< 0.05) for all metrics, confirming its good generalization ability. These results are consistent with those of the study by (Song et al., 2023), who used

https://doi.org/10.24191/jcrinn.v11i2.593

the radiomic approach with classical and ensemble algorithms and reported an AUC for the best of their models of 0.815 and 0.737 on the test set and corresponding accuracy of 0.716 and 0.747. While their models highlighted the effectiveness of textural and first-order statistical features, our study further extended this by incorporating the reproducibility of radiomic features using ICC analysis, thus ensuring consistency between scans, an aspect that has been less explored in previous work. Similarly, (Guo et al., 2021) implemented two models based on CT images and obtained respective AUCs of 0.840 and 0.789, with corresponding sensitivities of 0.813 and 0.838. In comparison, our model achieved AUCs of 0.937 and 0.907, and sensitivities of 0.755 and 0.889, which was a clear improvement, highlighting the need for the selection of consensus radiomic signatures and the use of hyperparameters obtained through systematic optimization. Kuang et al. (2024) developed interpretable models using SHAP analysis to predict three histological subtypes of NSCLC (ADC, SCC, LCC). Nine, twelve, and eight key radiomic features were selected for the ADC, SCC, and LCC groups, respectively. In terms of performance, the XGB model demonstrated superior performance in predicting SCC and LCC, with AUC values of 0.789 and 0.848, respectively. For ADC prediction, the Random Forest model excelled, with an AUC of 0.748. Unlike the study by Kuang et al. (2024) in our approach, Random Forest stood out from seven other classifiers, including XGB, and outperformed the authors' model with an AUC of 0.907 versus 0.789 for XGB for SCC prediction and 0.937 versus 0.748 for ADC prediction. Furthermore, the inclusion of the intraclass correlation coefficient (ICC) in our feature selection strategy enabled us to assess the stability and reproducibility of the features, in particular their robustness to inter-imaging-system variability. This step, which is also included in the methodology proposed by Kuang B. et al., enhances the reliability of the selected features and thus helps to improve the generalisability of our approach across clinical contexts and heterogeneous imaging environments.

In addition, other previous studies have combined multiple imaging modalities with tumor or biological markers, clinical information, and radiomic features to develop models for predicting histological subtypes of NSCLC. For example, Zhou et al. (2021) developed a radiomic signature from PET and CT images and implemented 45 prediction models based on nine machine learning algorithms. For the PET dataset, the Gradient Boosting Decision Tree (GBDT) feature selection method combined with a GBDT classifier achieved the best performance (AUC = 0.897), which was slightly lower than that of our model, whereas for the CT dataset, the best AUC (0.839) was obtained using GBDT selection combined with a Random Forest classifier, which was substantially lower than that of our model. Zhao et al. (2025) selected thirteen features, including nine radiomic features, two clinical features (gender and smoking status), and two biological markers (CEA and SCCA), and achieved an AUC of 0.910 on the test set. Finally, a few studies using deep learning have demonstrated the ability to predict subtypes: (Liang et al., 2024) developed a 3D CNN model for automatic feature extraction from computed tomography (CT) images. The results show that their proposed model achieved 0.88 accuracy and 0.89 area under the receiver operating characteristic curve (AUC) when distinguishing between ADC and SCC, indicating the potential for a non-invasive method to predict histological subtypes of lung cancer.

In our study, we constructed two separate prediction models for ADC and SCC, with respective AUCs of 0.937 and 0.907, and we further emphasized the ranking by importance of the consensually selected characteristics as well as the decision-making process of the models using the SHAP method. Our study rightly contributes to the reliable and accurate prediction of two histological subtypes of NSCLC. Furthermore, few studies have addressed the issue of data imbalance. The study of Lin et al. (2023), which did not address this imbalance, reported an AUC of only 0.700, well below that of our model. Thus, our work paves the way for the development of more reliable and accurate models in the future. Finally, given the "black box" nature of machine learning models (Petch et al., 2022), these models often lack interpretability in previous studies. Linning et al. (2019) developed a radiomic signature and implemented models to distinguish SCLC, ADC and SCC, obtaining AUCs of 0.822 and 0.665 respectively, but without providing any explanation of the ranking of features by importance or the decision-making process of the models. In our study, we implemented the SHAP method, which shed light on the decision-making process

https://doi.org/10.24191/jcrinn.v11i2.593

by providing a clear ranking of feature importance and illustrating how each feature influences decisions. This transparency is essential in a clinical setting, as it builds clinician confidence and facilitates understanding of the model's decision-making process. By revealing the contribution of individual radiomic features to the identification of ADC and SCC through SHAP strength diagrams, our approach improves the credibility of the models. This approach has further deepened our understanding of the link between radiomic features and tumor nature, paving the way for more personalized and effective therapeutic strategies. In this regard, we noted that ADC prediction depended mainly on global intensity and order 1 statistical features, especially after wavelet transformation. This shows a relatively homogeneous and structured grey-level distribution. In contrast, SCC prediction depended on complex textural features derived from GLSZM, GLRLM and NGTDM matrices, reflecting marked intratumorale heterogeneity and a more disordered spatial organization.

Compared with some previous studies and standard practices, our study had certain limitations. The first was that it was a retrospective, albeit multicenter, study, which potentially gave rise to selection bias, and that the number of patients in our cohort remained somewhat low, despite the large number of CT images collected in three different healthcare facilities and supplemented by public data. This reduced our ability to perform inter-center evaluations, which were essential for assessing the generalizability of our model's results across institutions and imaging protocols. Nevertheless, the large number of images allowed us to obtain valuable results using a bidirectional approach. Further efforts were needed to validate the robustness of the model and its applicability to new data. Secondly, manual segmentation of the regions of interest could lead to subjectivity and inter-operator variability, which could affect the robustness of the model. Thirdly, various CT scanners were used in the evaluation of patients, which resulted in inconsistent acquisition protocols between centers. Despite these limitations, we agreed with Zhao et al. (2025) that the diversity of the data accurately reflected everyday clinical practice in real-world settings. Therefore, a model trained on these data was expected to be more suitable for clinical implementation in real-world scenarios. For future work, we planned to expand the dataset through a larger prospective study encompassing a larger patient population, which would allow for comprehensive multicenter validation and the exploration of advanced algorithms, such as deep learning, feature fusion, and integrative approaches.

5. CONCLUSION

This study evaluated the potential of CT-based radiomics to non-invasively characterize histological subtypes of NSCLC. The discriminative performance of our RF model was satisfactory, demonstrating distinct radiomic signatures between adenocarcinoma and squamous cell carcinoma. Interpretability analysis based on the SHAP method identified the most contributory radiomic features and explained the decisions, thereby improving the transparency and confidence of the method. We believe that future work on larger prospective cohorts and the integration of multimodal data could improve the robustness and generalization of the model.

6. ACKNOWLEDGEMENT

The authors thank the hospitals, institutions, and colleagues who helped collect the data and support this study scientifically and technically, as well as the organizations that provided the public data used.

7. CONFLICT OF INTEREST DISCLOSURE

All authors declare that they have no conflicts of interest to disclose.

https://doi.org/10.24191/jcrinn.v11i2.593

8. AUTHORS' CONTRIBUTIONS

Christy Ntambwe Kabamba contributed to the conceptualisation, methodology, data analysis, and manuscript preparation; Tacite Mazoba Kpanya, a radiologist, contributed to data collection and preprocessing; Pierre Kafunda Katalayi and Angel Torrado-Carvajal contributed to the methodology, validation, and data analysis; Eugène Mbuyi Mukendi contributed to supervision, manuscript review, and editing. All authors have read and approved the final version of the manuscript.

9. REFERENCES

Aerts, H. J. W. L., Wee, L., Rios Velazquez, E., Leijenaar, R. T. H., Parmar, C., Grossmann, P., Carvalho, S., Bussink, J., Monshouwer, R., Haibe-Kains, B., Rietveld, D., Hoebers, F., Rietbergen, M. M., Leemans, C. R., Dekker, A., Quackenbush, J., Gillies, R. J., & Lambin, P. (2014). *Data From NSCLC-Radiomics (Version 4)* [Data set]. The Cancer Imaging Archive. https://doi.org/10.7937/K9/TCIA.2015.PF0M9REI.

Alahmari, S. S., Cherezov, D., Goldgof, D. B., Hall, L. O., Gillies, R. J., & Schabath, M. B. (2018). Delta radiomics improves pulmonary nodule malignancy prediction in lung cancer screening. *IEEE Access*, *6*, 77796-77806. https://doi.org/10.1109/ACCESS.2018.2884126.

Armato III, S. G., McLennan, G., Bidaut, L., McNitt-Gray, M. F., Meyer, C. R., Reeves, A. P., ... & Clarke, L. P. (2011). The lung image database consortium (LIDC) and image database resource initiative (IDRI): A completed reference database of lung nodules on CT scans. *Medical Physics*, *38*(2), 915-931. https://doi.org/10.1118/1.3528204.

Chen, T., & Guestrin, C (2016). XGBoost: A scalable tree boosting system. In *Proceedings of the 22nd ACM SIGKDD International Conference on Knowledge Discovery and Data Mining* (pp. 785–794). ACM. https://doi.org/10.1145/2939672.2939785.

Dirand, A. S. (2020). *Développements méthodologiques pour l'utilisation de caractéristiques radiomiques* [Doctoral dissertation, Université Paris-Saclay]. https://theses.hal.science/tel-03004812v1.

Eldho, K. J., & Nithyanandh, S. (2024). Lung cancer detection and severity analysis with a 3D deep learning CNN Model using CT-DICOM clinical dataset. *Indian J Sci Technol*, *17*(10), 899-910. https://doi.org/10.17485/IJST/v17i10.3085.

Esfahani, S. A., Torrado-Carvajal, A., Amorim, B. J., Groshar, D., Domachevsky, L., Bernstine, H., ... & Catalano, O. A. (2022). PET/MRI and PET/CT radiomics in primary cervical cancer: A pilot study on the correlation of pelvic PET, MRI, and CT derived image features. *Molecular Imaging and Biology*, *24*(1), 60-69. https://doi.org/10.1007/s11307-021-01658-1.

Fadzli, W. M. R. W., Dak, A. Y., & Razak, T. R. (2024). A survey on various edge detection techniques in image processing and applied disease detection. *Journal of Computing Research and Innovation*, *9*(2), 23-32. https://doi.org/10.24191/jcrinn.v9i2.415.

Guo, Y., Song, Q., Jiang, M., Guo, Y., Xu, P., Zhang, Y., ... & Yao, X. (2021). Histological subtypes classification of lung cancers on CT images using 3D deep learning and radiomics. *Academic Radiology*, *28*(9), e258-e266. https://doi.org/10.1016/j.acra.2020.06.010.

Hoffman, R. M., Atallah, R. P., Struble, R. D., & Badgett, R. G. (2020). Lung cancer screening with low-dose CT: A meta-analysis. *Journal of General Internal Medicine*, *35*(10), 3015-3025. https://doi.org/10.1007/s11606-020-05951-7.

Hu, G., Yang, Z., Zhu, M., Huang, L., & Xiong, N. (2018). Automatic classification of insulator by combining k-nearest neighbor algorithm with multi-type feature for the Internet of Things. *EURASIP Journal on Wireless Communications and Networking*, *2018*(1), 177. https://doi.org/10.1186/s13638-018-1195-1.

Kabamba, C. N., Mpuekela, N. L., Ntumba, B. S., & Mbuyi, M. E. (2019). Convolutional neural networks and pattern recognition: Application to image classification. *International Journal of Computer Science Issues (IJCSI)*, *16*(6), 10-18. https://doi.org/10.5281/zenodo.3987070.

Kim, J. W., & Shin, S. S. (2017). Ultrasound-guided percutaneous core needle biopsy of abdominal viscera: Tips to ensure safe and effective biopsy. *Korean Journal of Radiology*, *18*(2), 309-322. https://doi.org/10.3348/kjr.2017.18.2.309.

Kuang, B., Zhang, J., Zhang, M., Xia, H., Qiang, G., & Zhang, J. (2024). Advancing NSCLC pathological subtype prediction with interpretable machine learning: A comprehensive radiomics-based approach. *Frontiers in Medicine*, *11*, 1413990. https://doi.org/10.3389/fmed.2024.1413990.

Lambin, P., Rios-Velazquez, E., Leijenaar, R., Carvalho, S., Van Stiphout, R. G., Granton, P., ... & Aerts, H. J. (2012). Radiomics: Extracting more information from medical images using advanced feature analysis. *European Journal of Cancer*, *48*(4), 441-446. https://doi.org/10.1016/j.ejca.2011.11.036.

Liang, B., Tong, C., Nong, J., & Zhang, Y. (2024). Histological subtype classification of non-small cell lung cancer with radiomics and 3D convolutional neural networks. *Journal of Imaging Informatics in Medicine*, *37*(6), 2895-2909. https://doi.org/10.1007/s10278-024-01152-4.

Lin, J., Yu, Y., Zhang, X., Wang, Z., & Li, S. (2023). Classification of histological types and stages in non-small cell lung cancer using radiomic features based on CT images. *Journal of Digital Imaging*, *36*(3), 1029-1037. https://doi.org/10.1007/s10278-023-00792-2.

Linning, E., Lu, L., Li, L., Yang, H., Schwartz, L. H., & Zhao, B. (2019). Radiomics for classification of lung cancer histological subtypes based on nonenhanced computed tomography. *Academic Radiology*, *26*(9), 1245-1252. https://doi.org/10.1016/j.acra.2018.10.013.

Loh, W. Y. (2011). Classification and regression trees. *Wiley Interdisciplinary Reviews: Data Mining and Knowledge Discovery*, *1*(1), 14-23. https://doi.org/10.1002/widm.8.

Marentakis, P., Karaiskos, P., Kouloulias, V., Kelekis, N., Argentos, S., Oikonomopoulos, N., & Loukas, C. (2021). Lung cancer histology classification from CT images based on radiomics and deep learning models. *Medical & Biological Engineering & Computing*, *59*(1), 215-226. https://doi.org/10.1007/s11517-020-02302-w.

Nicholson, A. G., Scagliotti, G., Tsao, M. S., Yatabe, Y., & Travis, W. D. (2022). 2021 WHO classification of lung cancer: A globally applicable and molecular biomarker-relevant classification. *Journal of Thoracic Oncology*, *17*(9), e80-e83.

Petch, J., Di, S., & Nelson, W. (2022). Opening the black box: The promise and limitations of explainable machine learning in cardiology. *Canadian Journal of Cardiology*, *38*(2), 204-213. https://doi.org/10.1016/j.cjca.2021.09.004.

Pusztaszeri, M., Pache, J. C., Mach, N., Soccal, P. M., & McKee, T. (2011). Targeted therapy in lung cancer: Molecular testing using cytological specimens. *Revue Medicale Suisse*, *7*(303), 1486-1490.

Rastogi, S., Shrotriya, A., Singh, M. K., & Potukuchi, R. V. (2022). An analysis of intrusion detection classification using supervised machine learning algorithms on NSL-KDD dataset. *Journal of Computing Research and Innovation*, *7*(1), 124-137. https://doi.org/10.24191/jcrinn.v7i1.274.

https://doi.org/10.24191/jcrinn.v11i2.593

Robertson, S. E., Joyce, N. R., Steingrimsson, J. A., Stuart, E. A., Aberle, D. R., Gatsonis, C. A., & Dahabreh, I. J. (2024). Comparing lung cancer screening strategies in a nationally representative US population using transportability methods for the National Lung Cancer Screening Trial. *JAMA Network Open*, *7*(1), e2346295. https://doi.org/10.1001/jamanetworkopen.2023.46295.

Selvam, M., Sadanandan, A., Chandrasekharan, A. et al. (2024). Radiomics for differentiating adenocarcinoma and squamous cell carcinoma in non-small cell lung cancer beyond nodule morphology in chest CT. *Sci Rep 14*, 32088. https://doi.org/10.1038/s41598-024-83786-6.

Shukri, A. A. B., Yusoff, S. A. M., Warris, S. N., Bakar, M. S. A., & Kadar, R. (2024). machine learning approach of predicting airline flight delay using Naïve Bayes algorithm. *Journal of Computing Research and Innovation*, *9*(2), 140-155. https://doi.org/10.24191/jcrinn.v9i2.460.

Solodkiy, V. A., Nudnov, N. V., Karelidze, D. G., Borisov, A. A., Sultanova, P. N., Ivannikov, M. E., & Shakhvalieva, E. A. (2025). Determination of the histological type of lung cancer based on radiomic analysis of computed tomography chest images. *Medical Visualisation*, *29*(2), 29-38. https://doi.org/10.24835/1607-0763-1519.

Song, F., Song, X., Feng, Y., Fan, G., Sun, Y., Zhang, P., ... & Zhang, G. (2023). Radiomics feature analysis and model research for predicting histopathological subtypes of non-small cell lung cancer on CT images: A multi-dataset study. *Medical Physics*, *50*(7), 4351-4365. https://doi.org/10.1002/mp.16233.

Sung, H., Ferlay, J., Siegel, R. L., Laversanne, M., Soerjomataram, I., Jemal, A., & Bray, F. (2021). Global cancer statistics 2020: GLOBOCAN estimates of incidence and mortality worldwide for 36 cancers in 185 countries. *CA: A Cancer Journal for Clinicians*, *71*(3), 209-249. https://doi.org/10.3322/caac.21660.

Tang, X., Li, W., Sun, W., Wen, T., & Guo, K. (2025, May). Unbalanced data oversampling method based on improved VAE-CGAN. In *2025 5th International Symposium on Computer Technology and Information Science (ISCTIS)* (pp. 200-208). IEEE. https://doi.org/10.1109/ISCTIS65944.2025.11066045.

Van Griethuysen, J. J., Fedorov, A., Parmar, C., Hosny, A., Aucoin, N., Narayan, V., ... & Aerts, H. J. (2017). Computational radiomics system to decode the radiographic phenotype. *Cancer Research*, *77*(21), e104-e107. https://doi.org/10.1158/0008-5472.CAN-17-0339.

Yan, M., & Wang, W. (2020). Development of a radiomics prediction model for histological type diagnosis in solitary pulmonary nodules: the combination of CT and FDG PET. *Frontiers in Oncology*, *10*, 555514. https://doi.org/10.3389/fonc.2020.555514.

Zhao, J., Wang, T., Wang, B. et al. (2025). Deep learning radiomics fusion model to predict visceral pleural invasion of clinical stage IA lung adenocarcinoma: A multicenter study. Journal of Cardiothoracic Surgery, 20(1), 246. https://doi.org/10.1186/s13019-025-03488-6.

Zhou, Y., Ma, X. L., Zhang, T., Wang, J., Zhang, T., & Tian, R. (2021). Use of radiomics based on 18F-FDG PET/CT and machine learning methods to aid clinical decision-making in the classification of solitary pulmonary lesions: An innovative approach. *European Journal of Nuclear Medicine and Molecular Imaging*, *48*(9), 2904-2913. https://doi.org/10.1007/s00259-021-05220-7.

Zwanenburg, A., Vallières, M., Abdalah, M. A., Aerts, H. J., Andrearczyk, V., Apte, A., ... & Löck, S. (2020). The image biomarker standardization initiative: standardized quantitative radiomics for high-throughput image-based phenotyping. *Radiology*, *295*(2), 328-338. https://doi.org/10.1148/radiol.2020191145.

https://doi.org/10.24191/jcrinn.v11i2.593

https://doi.org/10.24191/jcrinn.v11i2.593

10. APPENDIX

REPUBLIQUE DEMOCRATIQUE DU CONGO
MINISTERE DE LA SANTE PUBLIQUE
COMITE NATIONAL D'ETHIQUE DE LA SANTE – CNES –

Arrêté Ministériel n°1250/CAB/MIN/S/ZKM/043/MC/2006 du 18 Décembre 2006
N° d'enregistrement au U.S. Department of health and Human Services (HHS) :IORG0008558/IRB
N° d'enregistrement au Federalwide Assurance (FWA) : 00026293

Avis du Comité National d'Ethique de la Santé n°620/CNES/BN/PMMF/2025 du 20/01/2025

Kinshasa, le 20 Janvier 2025

Au Mr. Christy NTAMBWE KABAMBA
Mention mathématiques, Statistiques et Informatique
Faculté des sciences et technologiques
Université de Kinshasa
Investigateur Principal

Concerne : Approbation éthique du protocole de recherche intitulé « Extraction des caractéristiques avec un modèle Deep Learning pour la détection du cancer bronchique à partir des images de tomodensitométrie à l'aide de l'approche ensemble Learning »

Monsieur le Principal Investigateur,

Le Comité national d'éthique de la santé a bien reçu votre lettre du 6 janvier 2025 par laquelle vous demandez l'autorisation de récolte des données médicales afin de réaliser votre projet de recherche doctorale dont l'intitulé est repris en concerne et vous remercie.

Après l'examen minutieux des aspects méthodologiques et éthiques de votre projet de recherche selon les lignes directrices nationales d'évaluation éthique de la recherche impliquant des sujets humains du Ministère de la santé de notre pays, le Comité National d'Ethique de la Santé a donné son approbation sur la méthode et les aspects éthiques de votre recherche.

Il autorise le déploiement de votre protocole de recherche aux Cliniques universitaires de Kinshasa, le Centre hospitalier Diamand, les Cliniques universitaires la renaissance et le Centre hospitalier Mére et Enfant de Monkole dans la ville de Kinshasa en République Démocratique du Congo pour la période allant du 20 Janvier 2025 au 19 Janvier 2026.

Veuillez agréer, Monsieur le Principal Investigateur, l'expression de nos sentiments les meilleurs.

Président du CNES
Prof. Félicien MUNDAY MULOPO

Siège Administratif : Immeuble PNMLS, 1er Niveau, Local 5, Commune de Kasa-Vubu -
Contact :(+243) 99 84 19 8 16, 0817670287, feli1munday @yahoo.fr. , Compte bancaire :
AFRILAND FIRST BANK CD- usd - cpte CNES N°00019 00001 02015196701 24 usd

https://doi.org/10.24191/jcrinn.v11i2.593